ASTRO-2022-B007

A Study on Asynchronous One-Way Ranging Scheme with Application to Deep Space Formation Flight

Junichiro Kawaguchi[1] and Masahiro Fujita[2]

The asynchronous one-way ranging scheme has been studied and developed by the authors. It successfully demonstrated the actual hardware verification recently. This helps small entities such as startups perform autonomous interplanetary missions avoiding heavy reliance on the agency assets. The scheme enables not only the range measurement but also the clock synchronization between two entities. It utilizes CDMA spread spectrum communication and is suitable for multiple paths among the formation.

The paper presents how effectively the scheme establishes the clock synchronization among the formation consisting of multiple spacecraft. And also, the paper extends and presents the idea on how the formation configuration is determined using the scheme. This will work and identify the configuration even in deep space, while it requires only uplink signal from the ground station on the Earth.

非同期 1Way 測距と深宇宙編隊飛行の航法への応用に関する一考察

川口 淳一郎 [1], 藤田 雅大（東大・院）[2]

月近傍ないし以遠における、レンジ計測を、簡易に行う方式として、著者らは、非同期 1 Way 測距方式を提案している。トランスポンダー方式では、折り返し遅延時間に光速をかけた距離の誤差を生ずるが、本方式での同期時間誤差は、レンジレートをかけた距離の誤差にとどまる点が最大の特徴であり、したがって、深宇宙での測距において、相互に同期を厳密にとる必要条件から解放できる点が最大の利点である。本報告は、この方式による測距試験結果および開発状況の報告を行うものであり、応用例とともに紹介するものである。

Introduction

Motivation & Objectives: Contemporary high demand of small spacecraft will extend to the deep space region performed even by Startups, Universities and small organizations. One potential obstacle for those activities is in navigation issue, since GNSS(GPS) is hardly available beyond GEO.

Current agency-provided services, range measurement facilities and flight dynamics support, and the

1. Australian National University (ANU), 2. Univ. of Tokyo

use of specifically defined analog-transponders will prevent autonomous operation by the small entities.

Solution and Benefit: One solution is what the paper presents: Avoiding the use of specific transponders, also avoiding agency-based facilities, this mutual dual asynchronous 1-Way communication method provides the small entities with autonomous range measurement and clock synchronization capability.

What is presented: Preliminary experiments performed using SDRs, and Development plan of the flight device. Measuring Formation Geometry and Clock Synchronization in Deep Space

Fig. 1 draws the typical principle about the GNSS. There is inevitably a time difference between the GNSS system clock and the use clock, and the travelling time read-out contains the error owing to the clock difference. The number of states to be estimated is three and the clock difference must be estimated at the same time. And the number of the observations should be larger than four.

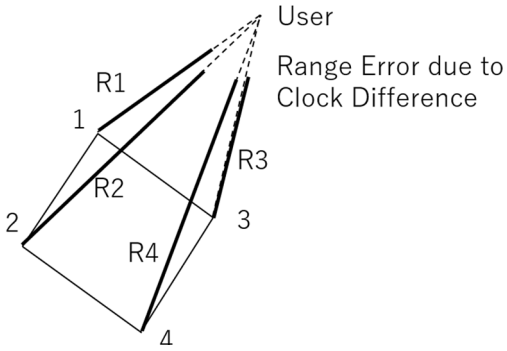

Fig. 1-a GNSS/GPS Measurements.

Here is begged a question: how many observations is required to estimate the clock difference. The answer is two. Since the distance or the range also affects the travelling time read-out, the clock difference must be estimated together with the distance between two entities.

Theoretical Background

The pseudo range obtained at t_s=t_3, onboard the spacecraft is

$$PR_{s/c} = -c\Delta t + R_3. \quad (1)$$

The pseudo range measured at t_g=t_5, at the ground station is

$$PR_{ground} = c\Delta t + R_5. \quad (2)$$

Denote PR_{ground} as y_g. y_g is rewritten as

$$y_g = c\Delta t + \frac{c}{c-\dot{R}_4}R_4^*. \quad (3)$$

When the time gap τ_s is introduced,

$$t_4 = t_3 + \tau_s, \quad (4)$$

y_g is re-expressed as

$$y_g = c\Delta t + \frac{c}{c-\dot{R}_3}\left(R_3 + \dot{R}_3\tau_s\right). \quad (5)$$

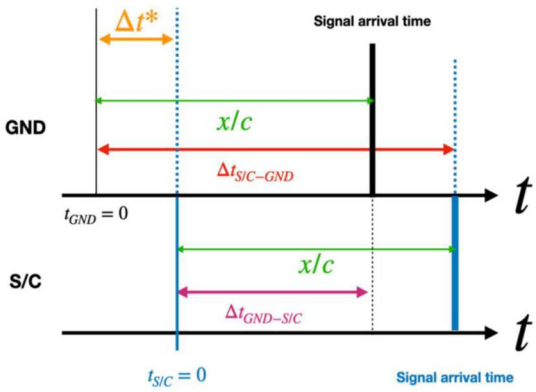

Fig. 1-b Asynchronous 1 Way Range

Assuming the range rate remains constant between t_3, both determine the range travelled at t_s=t_3 is

calculated by

$$R_3 = \left(\frac{y_s+y_g}{2} - \frac{1}{2}\frac{\dot{R_3}}{c-\dot{R_3}} c\tau_s\right) / \left(1 + \frac{1}{2}\frac{\dot{R_3}}{c-\dot{R_3}}\right). \quad (6)$$

The simplest property R_3 is approximately as

$$R_3 = \frac{y_s+y_g}{2}. \quad (7)$$

However, this may not be accurate enough, since the range rate deforms the range travelled and the time gap spent to relay degrade the measurement accuracy.

Once the R_3 is derived, the time difference becomes available for synchronization as

$$\Delta t = (R_3 - y_s)/c. \quad (8)$$

Differentiating the sum of the pseudo range information presents the approximated range rate as below.

$$\overline{\left(\frac{d}{dt}\frac{y_s+y_g}{2}\right)} / \left(1 + \frac{1}{2}\frac{\dot{R_3}}{c-\dot{R_3}}\right). \quad (9)$$

This property may be incorporated during the estimation process. The range R_3 accuracy relates to the uncertainty of the range rate as

$$\delta R_3 = \frac{1}{2}\left(\tau_s + \frac{R_3}{c}\right)\delta\dot{R} \quad (10)$$

It represents the feedback of the differentiation results. In order to avoid the instability, a low pass filter had better be incorporated.

Down Link Margin

Table-1 Down Link Margin.

Hardware Property	Unit	Cis-Lunar_Horn	1AU_Parabola
Frequency	MHz	8400 **(1W)**	8400 **(3.2W)**
TX Antenna		**Square Horn 9.2cm**	**Parabola 37.5cm**
(Efficiency)		**40deg Half Angle**	**η=0.5**
(Distance)	**km**	**421000 (Cis Lunar)**	**150 million (1AU)**
(Property)		**2.4m Diameter, η=0.7**	**12m Diameter, Parabola**
System Noise Temperature	dBK	23.6	23.6
RX G/T	dB/K	20.3	34.3
RX C/No	dBHz	35.7	15.7
Requirement Property			
Eb/No w/ margin	dB	9.6	9.6
Coherent Integration Gain	**dB**	**15**	**20**
(Property)		(1msec, 1MHz)	(10msec, 1MHz)
(Range Acquisition Rate)	**Hz**	**500 (1kHz/2)**	**50 (100Hz/2)**
Required C/No	dBHz	21.6	6.6
Link Margin	dB	14.1	9.1

Here is not shown, but the Up-link margin is well satisfied affordably by Startups, Universities and small organizations. Right Table assesses the down link margin analysis for micro and nano probes flying in cis-lunar and near Earth interplanetary regimes. Here is postulated the use of X-band. For cis-lunar flight, the ground station antenna is assumed 2.4m in diameter. And for 1 AU flight, it is assumed 12m in diameter. In this example, the transmission power aboard is assumed 1W and 3.2W for two type of flight respectively. Also here is assumed the onboard antenna are 9.2cm horn or 37.5cm dish for two types flights respectively.

GNSS/GPS Signal Availability

Taking the coding gain, the coherency integration gain, into account, even with small circular and plane 190mm antenna is practically usable in cis-lunar space, the link is assured, when range measurement frequency is lowered to 100Hz (Coding Gain).
This proves the GNSS(GPS) signal is acquired even by 6U-class nano-probes.

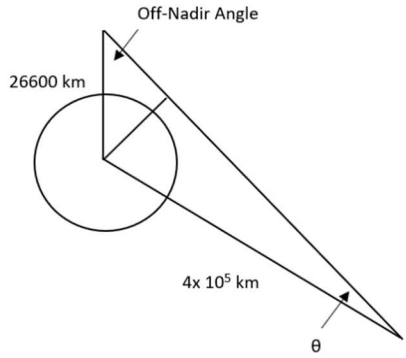

Fig. 2 Off-Nadir Angle of GNSS(GPS)

Table-2 GNSS/GPS Signal Availability

Hardware Property	Unit	Cis-Lunar_1kHz	Cis-Lunar_100Hz
Frequency	MHz	1575.42 **(23dBW)**	1575.42 **(23dBW)**
TX Antenna		**Off-Nadia Angle=20deg**	**Off-Nadia Angle=20deg**
		(-10dB w.r.t Zenith)	**(-10dB w.r.t Zenith)**
(Distance)	**km**	**421,000 (Cis Lunar)**	**421,000 (Cis Lunar)**
(Property)		**190mm Diameter, Zenith**	**190mm Diameter, Zenith**
System Noise Temperature	dBK	24.8	24.8
RX G/T	dB/K	-19.8	-19.8
RX C/No	dBHz	18.1	18.1
Requirement Property			
Eb/No w/ margin	dB	9.6	9.6
Coherent Integration Gain	**dB**	**15**	**20**
(Property)		(1msec, 1MHz)	(10msec, 1MHz)
(Range Acquisition Rate)	**Hz**	**500 (1kHz/2)**	**50 (100Hz/2)**
Required C/No	dBHz	21.6	6.6
Link Margin	dB	-3.5	11.5

Positioning Accuracy, Dilution of Precision in Cis-Lunar Space

Different from the LEO, the use of GNSS(GPS) for poisoning is never practical in cis-lunar space due to the extreme short baseline distance. Fig. 3 presents the Dilution Of Precision in ideal GNSS(GPS) satellites availability taking the off-Nadir restriction into account. Even in this case, as shown below, GDOP is significantly high.

Fig. 4 includes the limited GNSS(GPS) satellites availability. GDOP takes sky's limit.

However, if the clock synchronization is available, for instance, by this method, the positioning accuracy is assessed by PDOP instead. PDOP in the Table is still high, but is durable and usable.

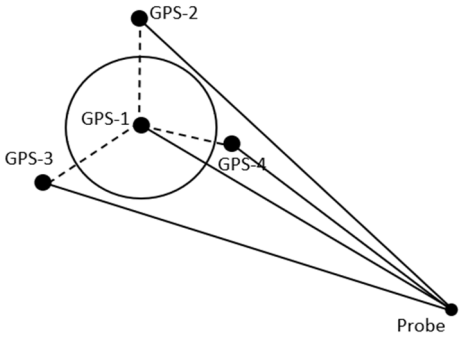

Fig. 3 No Side-Lobe Restriction

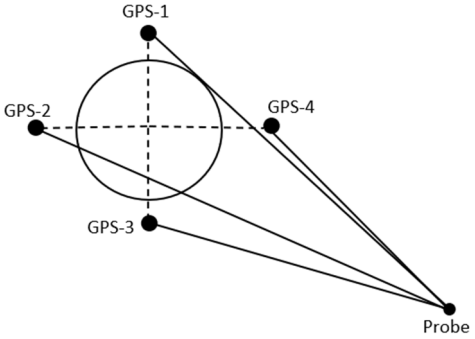

Fig. 4 With Side-Lobe Restriction

Table-3 GDOP and PDOP Comparison

Type		Earth Rim	IIR L1	Improved IIR-M L1	Improved IIR-M L1
Off-Nadir Angle (deg)		13.9	20	23	30
Configration-1 (Fig.3)	GDOP	12800	6300	4600	3000
	PDOP	70	60	40	35
Configuration-2 (Fig.4)	GDOP	N/A	10700	6200	9600
	PDOP	60	50	50	50

RF Wave Signal Distortion and its Spectrum

The RF signal transmitted still has instability when seen as CW, even in case 10MHz GPSDO stable clock is used. Left figure shows the peak-held RF signal that is obtained though rational multipliers. It exhibits 4-5 MHz fluctuation due to the distorted wave shape, while the frequency itself is accurately generated. Similarly, Right figure also shows the case in which 38.4MHz GPSDO clock is provided. The results also indicate the fluctuation. Besides, some sidebands appear possible due to the process in generating 38.4MHz.

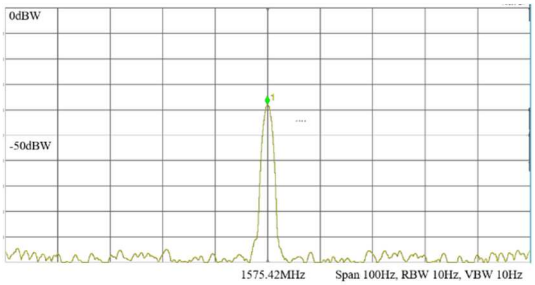

Fig. 5-a RF Fluctuation – GPSDO 10MHz

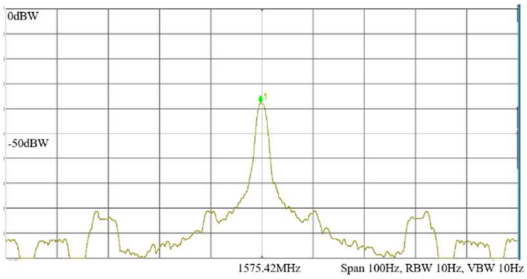

Fig. 5-b RF Fluctuation – GPSDO 38.4MHz

In principle, BladeRF runs based on the 38.4MHz and the fluctuation may not be unavoidable to output GNSS/GPS carrier of 1575.42MHz. The fluctuation directly affects to the pseudo range measurement error. 1Hz fluctuation causes 1nsec, 0.3m error.

As a side note, the similar peak-held spectrum density shows up to 150 Hz fluctuation when TCXO is used for BledeRF. (span 1kHz, RBW 10Hz, VBW 10Hz) See the figure below. It seems caused not only by the wave distortion but by the actual frequency drift. It should be noted the clock drift, even though it is large, is cancelled by the method presented here and the range measurement error does not appear.

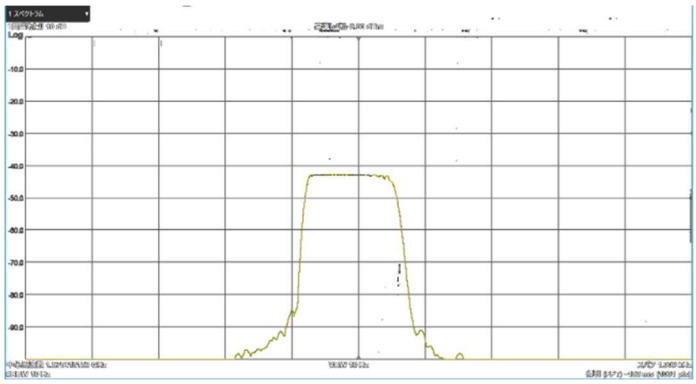

Fig. 5-c RF Fluctuation – TCXO

Wave Signal Distortion and its Effect to the Range and the Positioning

When the positioning is assessed using the GNSS/GPS simulator using the BladeRF, the following results were obtained. Here, the BladeRF is driven by the GPSDO clock.

Right figure shows the results using the real GNSS/GPS simulator that is not based on BladeRF. The positioning fluctuation is well suppressed. On the other hand, the positioning largely fluctuates when the simulator is built on the BladeRF. See left figure. The position drifts up to several meters. This may have been caused by the wave distortion rather than the frequency drift.

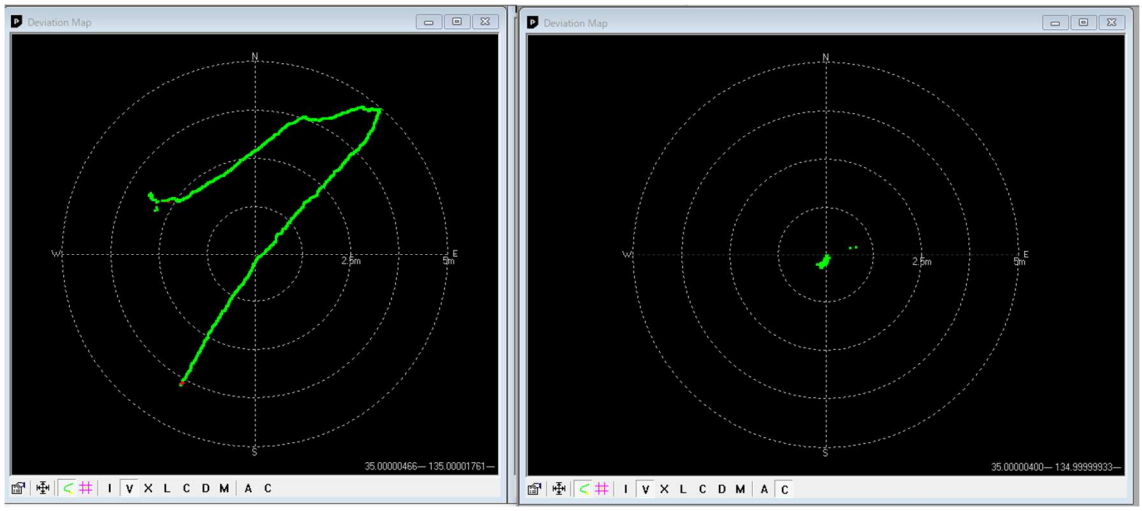

Fig. 6 Positioning Drift (BladeRF(left), Simulator(right))

Range Measurement Experiments Results

The figure below shows the range measurement stability when the self-loop-back test is conducted for about one minute. Here the absolute range measured has no meaning. There is observed a fluctuation of about 1.5m. It is estimated also caused by the wave distortion.

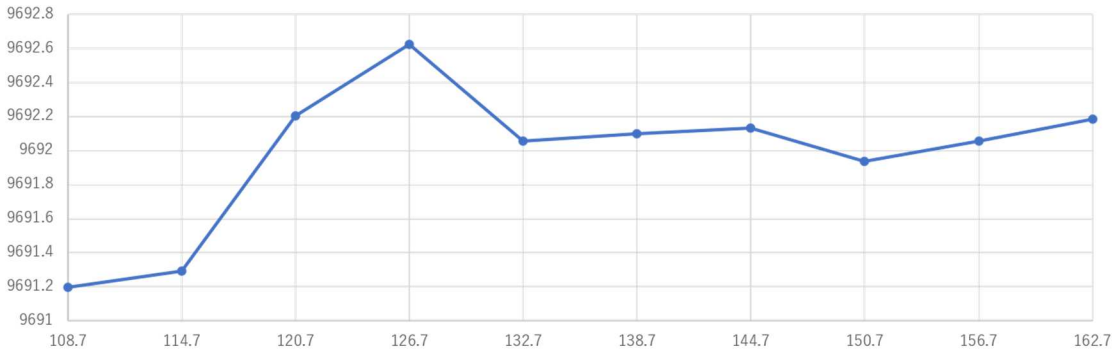

Fig. 7 Self-Loo-Back test results

The figure below presents the test results for the range and clock difference measurements. Here the distance is taken one million km with no range rate. The ground-station is driven by the GPSDO, while the spacecraft is driven by TCXO. Both runs and show the satisfactory accuracy of less than several meters as the theory says.

The measurements via asynchronous information exchange were obtained and listed below.

Table-4 Test Range Measurement results (ground-station, spacecraft)

	Range (GS側処理)	Δt (GS側処理)		Range (SC側処理)	Δt (SC側処理)
	補正後 range(m) GS側計測	Δt_RXsc,gs GS側計測(sec)		補正後 range(m) SC側計測	Δt_RXsc,gs SC側計測(sec)
438.700	999999999.8637	6.70971E-05	438.700		
444.700	1000000004.9539	6.76419E-05	444.700	1000000003.0314	6.764835E-05
450.700	999999998.8448	6.82196E-05	450.700	1000000001.5327	6.821068E-05
456.700	1000000004.7950	6.87656E-05	456.700	1000000001.3938	6.877693E-05
462.700	1000000000.1428	6.93362E-05	462.700	1000000004.1676	6.932278E-05
468.700	1000000003.6247	6.98882E-05	468.700	1000000000.1083	6.989989E-05
474.700	1000000001.1940	7.04478E-05	474.700	1000000004.4042	7.043710E-05
480.700	1000000003.6424	7.10250E-05	480.700	999999996.2134	7.104978E-05
486.700	1000000002.6776	7.16651E-05	486.700	999999999.3724	7.167615E-05
492.700	1000000003.6141	7.23060E-05	492.700	1000000004.9252	7.230162E-05
498.700	1000000002.0296	7.29864E-05	498.700	999999999.6145	7.299447E-05
504.700	1000000001.6592	7.37077E-05	504.700	999999995.9615	7.372667E-05
510.700	1000000002.9448	7.44282E-05	510.700	1000000000.7177	7.443569E-05
516.700	1000000002.0599	7.51516E-05	516.700	1000000001.7648	7.515264E-05
522.700	1000000002.5730	7.58606E-05	522.700	1000000007.1523	7.584533E-05
528.700	1000000002.9065	7.65528E-05	528.700	1000000007.3249	7.653808E-05
534.700	1000000002.9224	7.72452E-05	534.700	1000000003.4761	7.724337E-05
540.700	1000000000.6896	7.79487E-05	540.700	1000000001.0955	7.794731E-05

They are illustrated in Fig. 8-a, 8-b and 80c respectively below.

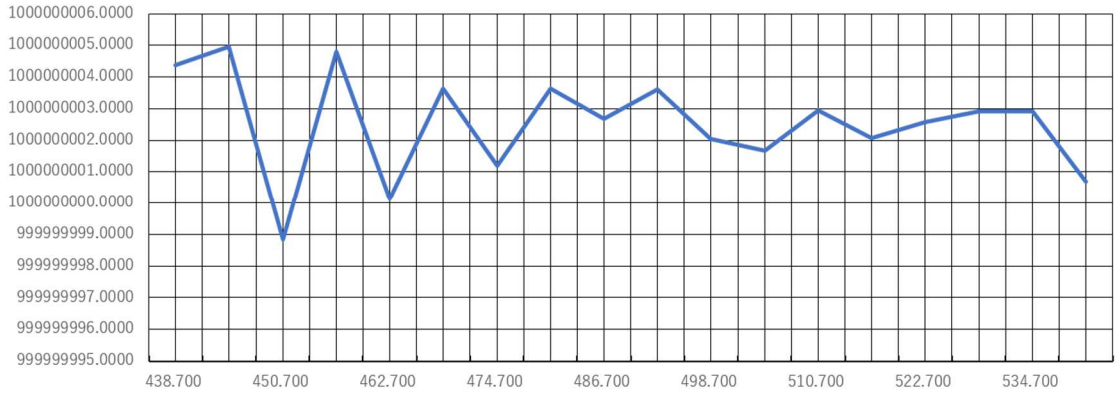

Fig. 8-a Range Measurement Results - ground station (10^6km)

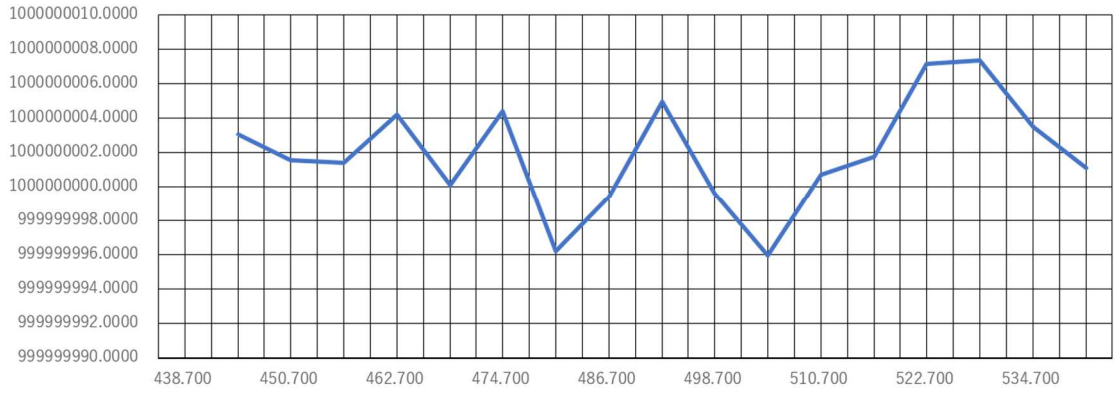

Fig. 8-b Range Measurement Results - spacecraft (10^6km)

Similarly, below the range measurement result is shown for the case of three million km.

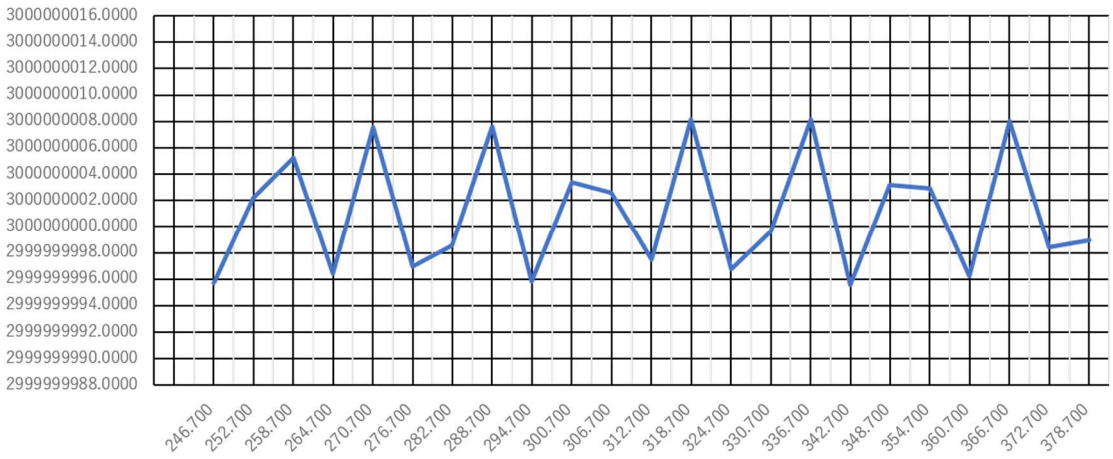

Fig. 8-c Range Measurement Results - ground station ($3x10^6$km)

Flight Demonstration and Test Hardware Development

Currently, the range measurement and clock synchronization experiments have been performed using SDR (BladeRF). The experiments simulate the delay by editing the transmission event time intentionally. So far, in the case of one million km, the accuracy of 30nsec, 10m is obtained.

In near future, the authors plan to have a flight demonstration using a 3U class CubeSat and are under preparation of 1.5U circuit boards with an onboard processor as shown below.

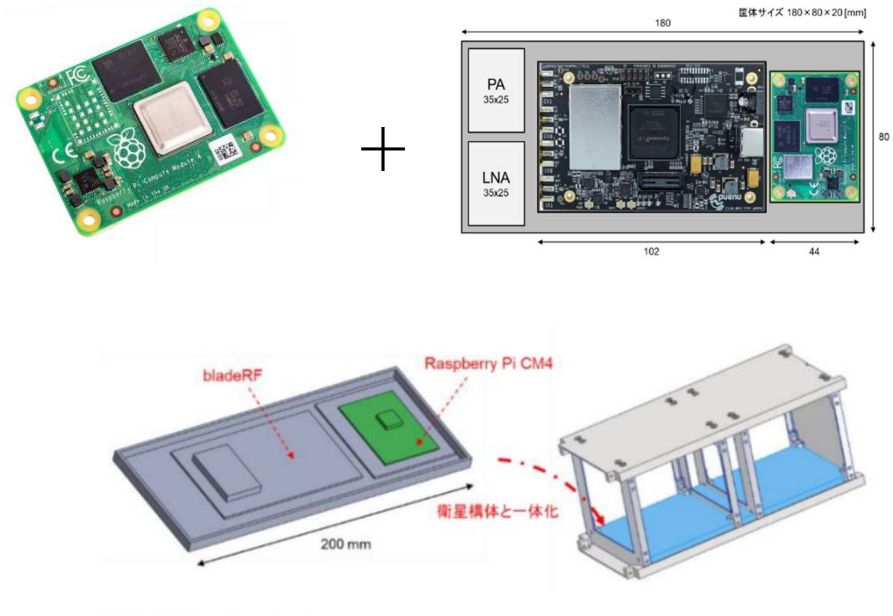

Fig. 9 Developing Flight Test Hardware

CONCLUSION

Mutual Asynchronous 1-Way Range Measurement Method was presented.

Mathematical analysis was provided.

Application to Positioning in Cis-Lunar space was discussed.

SDR-based BBM model was built for both Ground Station and Spacecraft.

Asynchronous Mutual 1-Way Transmission Experiment was performed.

- The range accuracy obtained for the case of 1 million km resulted in around 10m, while Time-Difference between Ground and Spacecraft was correctly excluded.
- This enables the clock aboard the spacecraft is synchronized within 30nsec w.r.t the clock on the Ground that is stabilized with GNSS(GPS).

Device Development plan was presented.

- Flight demonstration opportunities are expected.
- Hardware products should be available in future.

Device Development plan was presented.

- Notional Application to Deep Space Formation was discussed.

References

1) Willard Marquis, “The GPS Block IIR Antenna Panel Pattern and Its Use On-Orbit,” Proceedings of the 29th International Technical Meeting of the ION Satellite Division, ION GNSS+ 2016, Portland, Oregon, September 12-16, 2016. https://www.ion.org/publications/upload/GNSS16-0246.pdf
2) Anais Delepauta, et. al., "Use of GNSS for lunar missions and plans for lunar in-orbit development," Advances in Space Research, 2020, 66, 12, pp. 2739-2756, https://doi.org/10.1016/j.asr.2020.05.018
3) Jennifer E. Donaldson, Joel J.K. Parker, Michael C. Moreau, Dolan E. Highsmith, Philip D. Martzen, "Characterization of on-orbit GPS transmit antenna patterns for space users," NAVIGATION, Journal of the Institute of Navigation, 67, 2, pp 411-438, https://doi.org/10.1002/navi.361
4) Endrit Shehaj, Vincenzo Capuano, Cyril Botteron, Paul Blunt and Pierre-André Farine, “GPS based navigation performance analysis within and beyond the Space Service Volume for different transmitters’ antenna patterns,” Aerospace 2017, 4, 44. doi:10.3390/aerospace4030044
5) Shuai Jing, Xingqun Zhan, Jun Lu, Shaojun Feng and Washington Y. Ochieng, “Characterization of GNSS Space Service Volume,” THE JOURNAL OF NAVIGATION (2015), 68, © The Royal Institute of Navigation 2014, pp. 107–125.

doi:10.1017/S0373463314000472

6) Sehyun Yun, Kirsten Tuggle, Renato Zanetti & Christopher D'Souza, "Sensor Configuration Trade Study for Navigation in Near Rectilinear Halo Orbits," The Journal of the Astronautical Sciences, 2020, 67, pp. 1755–1774
7) Zhao-Yang Gao and Xi-Yun Hou, "Coverage Analysis of Lunar Communication/Navigation Constellations Based on Halo Orbits and Distant Retrograde Orbits," The Journal of Navigation, 2020, 73, 4, pp. 932 - 952, DOI: https://doi.org/10.1017/S0373463320000065
8) Shijun Xin, Yidi Wang, Wei Zheng, Yunhe Meng and Dapeng Zhang, "An Interplanetary Network for Spacecraft Autonomous Navigation," The Journal of Navigation, 2018, 71, 6, pp. 1381 - 1395, DOI: https://doi.org/10.1017/S0373463318000309
9) Jiri Skorepa, Pavel Kovar, Pavel Puricer, "PDOP parameters improvement using multi-GNSS and signal re-transmission at lunar distances," Advances in Space Research, Available online 30 June 2021, https://doi.org/10.1016/j.asr.2021.06.040
10) D. K. Shin, "Frequency and Channel Assignments." https://deepspace.jpl.nasa.gov/dsndocs/810-005/201/201D.pdf
11) "Near Earth Network (NEN) Users' Guide," 453-NENUG, Revision 4-Near Earth Network (NEN) Project, Code 453, NASA Goddard Space Flight Center, 2019. https://explorers.larc.nasa.gov/HPMIDEX/pdf_files/18_[Near_Earth_Network_(NEN)_Users'_Guide_Revision_4_Redacted_]453-UG-002905.pdf
12) Wang, Tianlin, Ruf, Christopher, Block, Bruce, McKague, Darren, Gleason, Scott, "Characterization of GPS L1 EIRP: Transmit Power and Antenna Gain Pattern," Proceedings of the 31st International Technical Meeting of the Satellite Division of The Institute of Navigation (ION GNSS+ 2018), Miami, Florida, September 2018, pp. 2879-2890. https://doi.org/10.33012/2018.16101
13) Peter Steigenberger, Steen Thoelert, and Oliver Montenbruck, "GPS and GLONASS Satellite Transmit Power: Update for IGS repro3," Technical Note, DLR/GSOC TN 19-01, 11 July 2019.